The growth and optical properties of large, high-quality AlN single crystals

Martin Strassburg,[a] Jayantha Senawiratne, and Nikolaus Dietz
Department of Physics and Astronomy, Georgia State University, Atlanta, Georgia 30303-3083

Ute Haboeck and Axel Hoffmann
Institute of Solid State Physics, Technical University of Berlin, 10623 Berlin, Germany

Vladimir Noveski, Rafael Dalmau, Raoul Schlesser, and Zlatko Sitar
Department of Material Science and Engineering, North Carolina State University, Raleigh, North Carolina 27695-7919

The effect of impurities and defects on the optical properties of AlN was investigated. High-quality AlN single crystals of more than 20 mm^2 size were examined. Different crucible materials and growth procedures were applied to the growth of bulk AlN by physical vapor transport method to vary the defect and the impurity concentrations. The crystalline orientation was investigated by Raman spectroscopy. Glow discharge mass spectrometry was used to determine the trace concentration of the incorporated impurities such as oxygen and carbon. The photoluminescence emission and absorption properties of the crystals revealed bands around 3.5 and 4.3 eV at room temperature. Absorption edges ranging between 4.1 and 5.95 eV were observed. Since no straight correlation of the oxygen concentration was obtained, a major contribution of oxygen or oxygen-related impurities was ruled out to generate the observed emission and absorption bands in the Ultraviolet spectral range. The carbon-related impurities and intrinsic defects might contribute to the observed optical properties. The absorption coefficient for AlN single crystals has been derived for the spectral range below the band edge. © *2004 American Institute of Physics*. [DOI: 10.1063/1.1801159]

I. INTRODUCTION

The unique properties of the group III-nitrides, such as wide direct band gap, high thermal conductivity, and high thermal stability have made GaN and AlN the most serious candidates for the high-power and high-frequency electronic and deep ultraviolet (UV) optoelectronic devices.[1,2] Nevertheless, the full potential of these devices has been limited by the challenge to produce high-quality group III-nitride layers and crystals. The present insufficient quality is attributed to a high density of crystal defects, mainly dislocations ($\sim 10^8 - 10^{10}$ cm^{-2}) that originate from the substrate and from the growth process due to thermal and lattice mismatch between the substrate and overgrown group III-nitride thin films.[3,4] A significant reduction of dislocation density is mandatory to further improve the device performance. The use of AlN bulk crystals as substrates in the group III-nitride device fabrication process is expected to yield substantially reduced dislocation densities (below 1000 cm^{-2}) by minimizing the defects from the substrate and by reducing the lattice and thermal mismatch.[5–7] Therefore, the growth of bulk AlN crystals is of primary importance for the development of III-N-based devices with improved characteristics and extended lifetime. Additionally, AlN intrinsically has a high resistivity and is, therefore, a very suitable substrate for microwave applications.

Reliable measurements of the properties of AlN are hard to find. This is particularly due to a general lack of an appropriate growth procedure to achieve sufficiently large AlN single crystals with reproducible high quality. The sublimation, vaporization, and melts have been used as a source supply in the growth of bulk AlN crystals.[8–10] Physical vapor transport (PVT) by powder sublimation[5–14] has yielded the most promising results. However, this technique requires very high process temperatures exceeding 2000 °C. A similar method has been proven to grow high-quality SiC, which has similar structure and growth parameters as AlN. In this work, the PVT method was used to grow AlN bulk crystals by sublimation of AlN powder in a nitrogen atmosphere at growth temperatures of 1800–2400 °C and pressures of 400–600 Torr.

Several analytical and experimental studies of the physical properties of AlN have been reported in the literature. Spectroscopic measurements in the UV, visible, and IR range have been published.[15] Theoretical calculations and experimental absorbance studies in the UV range determined that AlN has a direct band gap somewhere between 5.8 and 6.2 eV [at room temperature, (RT)] and 6.28 eV (at 5 K).[15–18]

Oxygen is a commonly encountered impurity in the AlN crystals, and previous studies investigated its influence on the growth kinetics[19] as well as the optical properties as characterized by the luminescence, absorption,[20–26] and Raman spectroscopy.[25] The observed broad emission bands in the midgap range from 3.5 to 4.5 eV have been attributed to the presence of oxygen.[20,23,24] The octahedral inclusions formed by oxygen atoms in AlN crystals have been observed at high

[a]Author to whom correspondence should be addressed: Georgia State University, 29 Peachtree Center Avenue, Suite 408, Atlanta, GA 30303-3083; FAX: (904) 651-1427; electronic mail: mstrassburg@gsu.edu

oxygen concentrations above 10^{21} cm^{-3}.[23] An absorption peak between 2.8 and 2.9 eV has been assigned to nitrogen vacancies acting as shallow donors.[20,23,27] The emission and absorption bands around and below 2.5 eV have been attributed to the point defects such as nitrogen vacancies and Al atoms on interstitial sites.[28–32] Although near-band-gap luminescence features have been assigned to exciton recombination, either from the free excitons or from the excitons bound to various shallow donors or acceptors (e.g., Ref. 23), an allocation of near-band-edge states to certain impurities and crystal defects has not been presented yet.

Optical investigations of wurtzite AlN in the IR range have yielded average values for the dielectric constant and the refractive index of about 4.77 and 2.18,[15] respectively. Literature values of the refractive index range between 1.99 and 2.55, whereas the high- and low-frequency dielectric constants have been reported in the ranges of ε_∞ $=4.68-4.84$, and $\varepsilon_0=8.3-11.5$, respectively. These results have been obtained by the general Lyddane-Sachs-Teller expression, which accounts for the contribution of phonons to the optoelectronic properties of the materials.[33] The *ab initio* calculations, as well as the experimental Raman data have yielded information on the density of states and the dispersion of phonons in wurtzite AlN crystals.[34,35] TO and LO modes have been observed at 667 cm^{-1} and at 905 ± 12 cm^{-1}, respectively, using Raman spectroscopy.[34,36–40] The E_2 mode has been observed at 665 and 657 cm^{-1}[16,36] (in the Γ point of the Brillouin zone). Due to the lack of high-quality single AlN crystals, the complete $\omega(k)$ phonon-dispersion relations have not been determined by inelastic neutron-scattering techniques thus far.

This paper discusses the influence of common impurities in the bulk AlN crystals on the absorption, luminescence, and Raman-scattering properties. Varying levels of impurities and defects in the AlN crystals characterized in this work resulted from different process conditions and the use of different reaction crucibles in the PVT process. The glow discharge mass spectrometry (GDMS) was applied to determine the concentrations of contaminants in the crystals. These are compared to the optical absorption and photoluminescence properties, and the influence of oxygen and other impurity-related defects to the absorption, band gap, and lattice vibrations is investigated.
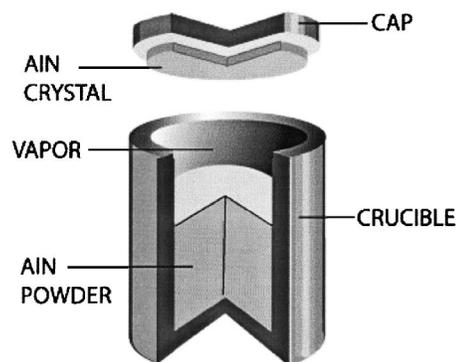
FIG. 1. Growth of AlN bulk crystals: Sandwich-sublimation configuration.

II. EXPERIMENT

A PVT process was used to grow bulk AlN crystals by sublimation of AlN powder in an ultrahigh purity nitrogen ambient. The growth was performed in two reaction systems, a resistively heated[5,6] and an inductively heated reactor configuration.[41,42] In the typical sandwich-sublimation configuration employed in this work, the bulk crystal growth takes place in a reaction crucible, as shown in Fig. 1. The AlN powder sublimes from the bottom of the crucible, which is kept at a relatively higher temperature, forming gaseous species of Al and N_2. These species are then transported through the vapor phase to the top of the crucible, where the crystal grows by recrystallization at a relatively lower temperature. The capped, cylindrical crucibles made of BN, TaC, and TaN with inner diameters of 1.0–1.25 in. and 2.5 in.-long were used in the growth experiments. Different crucible materials and varying growth parameters yielded the bulk AlN crystals with different concentrations of impurities. These samples were used for analyzing the effects of impurities and of impurity-related defects in the bulk AlN crystals on the physical properties of AlN. Table I summarizes the growth conditions of the four samples, randomly chosen for this study.

Four samples labeled respectively as A, B, C, and D are presented. These crystals had cross-sectional areas above 10 mm^2 with an exception of sample C ($\sim 1.5 \times 2$ mm^2). The concentrations of impurities in these crystals were measured by GDMS and the results for the four samples are summarized in Table II.

TABLE I. Summary of Physical vapor transport (PVT) growth conditions.

Sample	A	B	C	D
Reactor	Resistively heated	Resistively heated	Inductively heated	Inductively heated
Substrate	Spontaneous nucleation	MOCVD-coated 6H-SiC with $\sim$330 nm AlN	Polycrystalline AlN from self-seeded growth	Polycrystalline AlN from Self-seeded growth
Crucible	BN	TaN	TaC	TaC
Source	Al(metal)+AlN	AlN powder	Sintered AlN powder	Sintered AlN powder
Crystal T (°C)	1950/2070[a]	1885/2030[a]	2100	2100
Source T (°C)	2070/2200[a]	2010/2155[a]	2110	2110
Pressures (Torr)	500/400[a]	600/600[a]	500	500
T gradient (°C/mm)	3	2.5	1	1
Time (h)	2/13	16/17	16	50

[a]Samples A and B were grown using a two-stage growth process; temperatures were gradually ramped between the two stages.

TABLE II. GDMS analysis of the impurity content in AlN crystals (ppm wt).

Sample	A	B	C	D
Element	Concentration (ppm wt.)	Concentration (ppm wt.)	Concentration (ppm wt.)	Concentration (ppm wt.)
B	100	28	0.11	0.77
C	$\leqslant 300$	$\leqslant 160$	$\leqslant 50$	$\leqslant 30$
O	$\leqslant 500$	$\leqslant 1200$	$\leqslant 50$	$\leqslant 400$
Si	5.5	130	40	40
Mn	<0.05	0.23	<0.05	<0.05
Fe	<0.1	2.4	<0.25	0.35
Cr	1.1	0.3	<0.1	<0.1
W	<1	<0.05	<1	<1
Ir	<0.5	<0.05	<0.5	<0.5

III. OPTICAL INVESTIGATIONS ON ALN SINGLE CRYSTALS: RESULTS AND DISCUSSION

Photoluminescence (PL) and transmission spectroscopy were performed to analyze the emission and absorption properties of AlN bulk crystals, whereas Raman spectroscopy was employed to investigate the lattice dynamics and the structural crystal quality. Transmission spectra of the crystals were recorded between 6.46 eV and ~10 meV (192 nm and 500 μm), allowing an investigation of the band-edge transition in the UV range, the impurity transition bands in the visible range and in the near infrared (NIR) range, as well as the phonon bands and the Reststrahlen band ($\geqslant 10\ \mu$m) in the far infrared (FIR) range. Different light sources (deuterium-, XBO-, halogen, and filament lamps) were applied for the respective spectral ranges. The transmitted light was detected by a photomultiplier (Hamamatsu R955), InGaAs-, InSb-, HgTe-MCT, and a tryglycine sulfate detector, respectively. Several optical edge filters and beam splitters were applied to suppress the excitation of luminescence via the ban-edge or states in the band-gap having higher energies. A more detailed description of the experimental setup applied for the FIR investigations is presented elsewhere.[43]

Raman experiments were performed in a backscattering geometry with a triple-grating spectrometer and cooled charge-coupled device detector. The 632.8 nm line of He–Ne laser was used for excitation. The line positions were determined with an accuracy better than 1 cm^{-1}. The PL of the samples was excited by the fourth harmonic of a Ti:sapphire laser (λ=210 nm). The emitted light was detected by a photomultiplier (Hamamatsu R955) attached to a 0.25 m monochromator. The spectral resolution of the system was better than 1 nm.

The near-band-edge transmission facilitates a determination of the effective bandedge and hence allows an assessment of the optical quality of the crystals. In Fig. 2, the transmission spectra of the AlN bulk samples are shown for the UV and visible spectral range. According to the onset of the transmission, sample B has the highest optical quality, indicating the smallest amount of shallow impurities and defects. The onset of the transmission for sample B starts at 5.9 eV (~210 nm), whereas the onset of the transparency in the other crystals starts below 4.96 eV (above 250 nm, #A) or even more redshifted at 4.13 eV (~300 nm, #C). The transparency threshold of the respective samples was determined from the transmission behavior, and the values are summarized in Table III. Between 4.13 and 2.5 eV (300 and 500 nm), the transmission increases in all the samples and remains nearly constant at a maximum value until ~250 meV (~5 μm), not shown here. The significant reduction of the transmission signals below the bandgap can be assigned to the electronic states introduced by the native defects and impurities, as discussed in more detail subsequently.
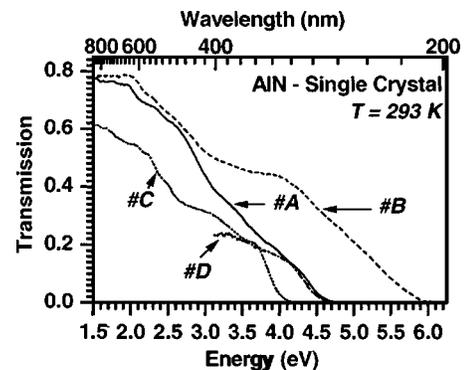
FIG. 2. Transmission behavior of AlN bulk single crystals in the visible and UV spectral range.

TABLE III. Specific properties of the AlN single-crystal samples. The energy of the transparency edge was determined from the slope in band tailing of the transmission spectra.

Sample	A	B	C	D
Single crystalline area (mm^2)	30	25	3	12
Color	transparent	transparent	light brown	light brown
Thickness (μm)	530	140	670	920
Absorption edge at RT(eV)	4.7	5.95	4.1	4.7
Orientation	(0001) axis in plane	(0001) axis perpendicular to the plane	random	12° off the (102) plane
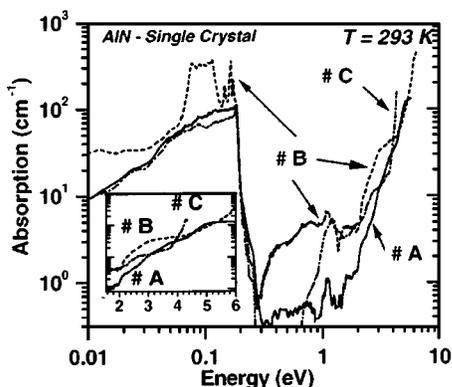
FIG. 3. Absorption coefficient as a function of energy for the AlN bulk samples A, B, and C. The inset depicts the UV and visible spectral range on a linear energy scale.

The spectral absorption coefficient has been computed from the transmission data below the bandgap using literature data for the dispersion of the refractive index.[18] Corrections for the reflection loss at the interfaces (air/AlN and AlN/air) were included. In addition, the Sellmeier equation[44] was applied to derive the refractive index of AlN as a function of wavelength in the region close to the bandgap. The applied fitting parameters (including the dispersion of the refractive index) were taken from the data reported by Brunner *et al.*[18] Hence, the absorption coefficients were determined for the spectral range from the UV (near band edge) through the far infrared region. We note that the accuracy of the refractive index is limited in the UV and in the IR (>3 μm) spectral range due to the applied fitting parameters in the Sellmeier equation. The deviation is by far stronger in the UV spectral range because the refractive index increases near the band edge, while it remains nearly constant in the IR. Laws *et al.*[45] have shown that for the AlGaN material system, the deviation of the refractive index in the UV spectral range crucially depends on the determination procedure of the fitting parameters for the Sellmeier equation. Moreover, near the band edge, the excitonic oscillations and defect-induced electronic transitions are known to significantly modulate the refractive index.

In Fig. 3, the respective absorption coefficients as a function of energy (wavelength) are shown for the AlN bulk samples. While the absorption coefficient decreases continuously in the visible and NIR spectral range, a minimum (<5 cm^{-1}) is observed between 300 meV and 1.8 eV. Below 300 meV, a steep increase in the absorption coefficient is observed reaching the values close to that near the band edge. Different absorption peaks in the NIR range were observed only for sample B. These absorption structures have been assigned to the phonons in wurtzite AlN crystals. Meanwhile, the absorption spectra of the other samples did not allow a clear definition of the absorption bands in the NIR range.

The analyzed AlN bulk crystals exhibited an increased absorption at energies approaching the band gap of AlN. In fact, the maximum values of the absorption coefficients, in the order of several hundred cm^{-1} were located near the band edge. The negative deviation between these values and the

literature-reported absorption coefficients of $\sim 10^5$ cm^{-1}, Refs. 18, 46, and 47 confirmed the viability of the PVT process for the growth of AlN bulk crystals with a better UV transparency as compared to the thin metal-organic chemical-vapor deposition layers. The limited validity of the Sellmeier equations, especially in the range of free and bound excitons, may have introduced an additional error resulting in an underestimation of the absorption coefficients.[26,48,49] In addition, emission and scattering processes at the crystal surface may also introduce inaccuracy in estimation of the absorption coefficients. We note that in more recent publication, theoretical values smaller than 10^4 cm^{-1} have been reported as well.

In the visible and UV range, absorption bands were observed at 2.3/2.5, 3.0 and 5.1 eV. The first band is assigned to a resonant absorption in deep defects, being responsible for the "yellow luminescence" (YL). The latter is associated in literature with oxygen- and vacancies-related defects.[20–26] These bands will be discussed in more detail subsequently, with the analysis of the midgap luminescence of AlN.

Small values for the absorption coefficients (<5 cm^{-1}) were estimated in the near- and mid-IR spectral range. At these photon energies (<1.6 eV), all the crystals are almost completely transparent, confirming an insignificant contamination of the samples with transition metals and rare-earth elements.

A pronounced increase in the absorption coefficients was detected below 300 meV (above 5 μm), indicating the onset of a resonant absorption of light by phonons.[36–38] While broad absorption bands dominated the spectra of most of the samples, spectrally well-defined absorption peaks were resolved for the sample B. These peaks were assigned to the resonant single and multiphonon absorption processes.[34]

High absolute values of the estimated absorption coefficients at low energies may be assigned to the modulation of the refractive index according to the Reststrahlen band,[50,51] which was not taken into account in this study. Thus, no quantitative value of the absorption coefficient is given for this spectral range. More attention is drawn to the far IR absorption bands of AlN single crystals by analyzing the optical and acoustic phonons revealed in sample B.

Raman spectroscopy was applied to assess the structural quality and orientation of the AlN crystals by analyzing the phonon frequencies. Figure 4 shows the Raman spectra of crystals A and C. The E_2(low) mode at 246 cm^{-1} (31 meV), the A_1(TO) mode at 609 cm^{-1} (76 meV), the E_2(high) mode at 655 cm^{-1} (81 meV) the E_1(TO) mode at 668 cm^{-1}(83 meV), and E_1(LO) mode at 911 cm^{-1} (113 meV) were revealed. The mode energies are in good agreement with the absorption bands in the FIR published for the unstrained AlN.[34] The pronounced shift of the A_1(TO) mode and the broadening of all the Raman modes in the spectra of sample C were attributed to its undefined orientation. The single crystalline grain (sample C) was sliced from a cross section of a polycrystalline boule, grown by utilizing the grain expansion in the direction of growth.[42] However, a higher defect-induced charge-carrier concentration and the presence of strain due to constraints imposed by the competition between the multiple grains cannot be ruled
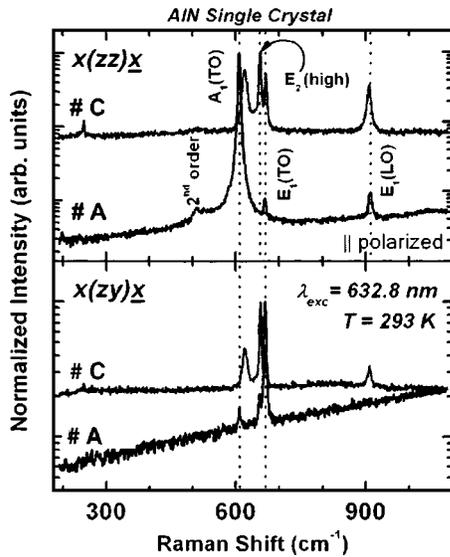
FIG. 4. Raman spectra of the AlN single-crystal samples A and C. According to the tested selection rules, either the A_1(TO) mode or the E_1(TO) mode govern the spectra of #A, demonstrating the high-crystalline orientation of this sample. Superposition, shift, and broadening of the Raman modes of sample C are caused by its less-crystalline orientation and quality.

out. Moreover, the LO mode around 655 cm^{-1} shows neither A_1 nor E_1 symmetry and is therefore labeled as a quasi-LO mode. Applying the selection rules, the structural quality was evaluated. The $x(zz)x$ geometry was chosen because in this geometry, the A_1(TO) mode and the E_1(TO) mode are allowed, whereas the E_2(high) mode is forbidden for sample A. By contrast, in $x(zy)x$ geometry, the A_1(TO) mode is suppressed and the spectrum is governed by the E_1(TO) mode. The Raman spectra of sample A (see Fig. 3) confirm these predictions indicating the good structural quality and (0001) orientation of the crystal. The detected superposition of A_1(TO), E_2(high), E_1(TO), and E_1(LO) modes for the sample C indicated an inhomogeneous orientation of this crystal. This was also supported by x-ray diffraction (XRD) (using a two-dimensional detector system by Bruker AXS/GADDS), which confirmed that the top surface of sample C formed an angle of ~12° relative to the (11–20) crystallographic plane of wurtzite AlN (see also Table III). However, contrary to the Raman spectra XRD analysis showed the single-crystalline nature of the sample, with full width at half maximum of less than 0.5° on (11–20) rocking curve. This indicated that the structural quality of randomly oriented AlN crystals cannot be successfully evaluated by analyzing the optical and acoustic phonons off the Γ point by Raman spectroscopy. A more accurate analysis would require determination of the polarization vector and the single-crystal orientation relative to the (0001) direction.

The PL spectroscopy was performed to provide an additional assessment of the optical quality and better insight to the influence of the crystal defects and native impurities on the optical properties of the bulk AlN crystals. The observed absorption and emission bands facilitated the identification of the possible active contaminants and defects in the crystals. A summary of the PL results for the analyzed samples is shown in Fig. 5. Due to technical limitations, the maximum
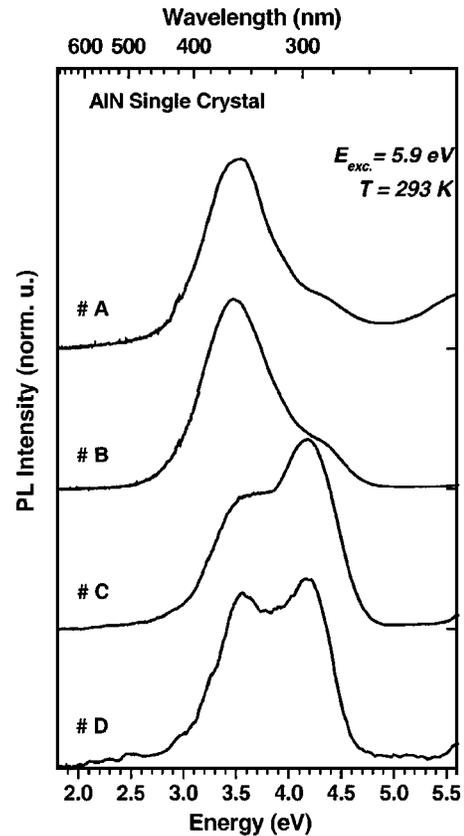
FIG. 5. Photoluminescene (PL) as a function of emission energy for all the investigated AlN bulk samples.

excitation energy was 5.9 eV (210 nm) and hence, no information about band-to-band transitions could be extracted. The luminescence above 5.6 eV (below 222 nm) was not evaluated because of the superposition of scattered laser light and resonant near-band-edge emission.

A broad luminescence band having energies well below the band gap was observed in all the samples. An emission band around 4.43 eV (280 nm) was resolved. It was found to govern the spectrum in sample C, which showed a reduced optical transmission in the UV and in the visible spectral range. In sample D, two emission peaks of nearly the same intensity were detected at 4.43 eV (280 nm) and at 3.44 eV (360 nm). The PL maximum of the other AlN samples was found to be more redshifted. The spectra of #A and #B were governed by the defect bands peaking at 3.55 eV (360 nm) and 3.44 eV (3.49 nm). Further peaks were observed at 3.93 eV (315 nm), 4.73 eV (262 nm), and 4.88 eV (254 nm), being most pronounced in crystals #A and #D.

The emission peaks around 3.5 eV are attributed to the oxygen-related impurities.[20,25,52,53] Youngman and Harris[20] found that with an increasing oxygen concentration, the emission peak energy shifts to lower energies. Despite varying oxygen concentrations (from 50 ppm in sample C until 1200 ppm in sample B), no significant change in the peak energy of the investigated samples were detected. We note that the well-defined, clear absorption peak around 4.43 eV(280 nm), which is in absorption, but not in the PL assigned to oxygen-related defects, was not detected in

J. Appl. Phys., Vol. 96, No. 10, 15 November 2004

Strassburg *et al.* 5875

sample B. However, a pronounced emission band around 3.5 eV governed the PL spectrum of this sample. The comparison of the obtained PL spectra with the elemental analysis data (GDMS, see Table II) rules out that oxygen alone is generating this emission band. The sample with the highest concentration of oxygen inherited the smallest absorption coefficients in the whole UV range, and the emission band around 3.5 eV detected in all the samples is not correlated with the detected oxygen concentration. Hence, other impurities or defect centers need to be considered as possible culprits for these transitions. The GDMS analysis revealed that in addition to O, Si and C were present in the crystals at concentrations that may have a significant influence on the luminescence properties of AlN. In carbon-doped AlN films, C or C-related defect complexes may cause impurity states with respective transition energies around 4.4 eV.[54] However, in this study, no straight correlation was detected between the C concentration and the dominance of this PL peak.

An additional peak was observed around 2.95 eV (420 nm) in all crystals. These broad emission bands were found to consist of several overlapping peaks between 3.55 eV (349 nm) and 2.7 eV (458 nm).[28–31] It is speculated here that these bands could be assigned to the nitrogen vacancies or interstitial Al (3.55 and 3.33 eV). The peak around 2.8 eV is typically only observed in samples with low oxygen content and disappears once the oxygen exceeds 6×10^{20} cm^{-3}. It is interesting to note that using a defect equilibrium formulation, an expression can be derived showing that the concentration of oxygen is inversely related to the concentration of nitrogen vacancies.[55] Based on the growth procedure (SiC-seeded technique), the presence of vacancies and native defects in crystals #A and #B should be somewhat higher than in #C and #D (self-seeded growth and AlN-seeded techniques). However, this could not be resolved unambiguously by the present study.

In addition, emission peaks that were detected around 2.2 eV (580 nm) had a significantly lower intensity. They were merged and contributed to the observed broadband emission described earlier. A slight change in their relative intensities was observed in the investigated samples. Based on the analogy with GaN[56,57] and theoretical predictions,[58] these bands have been attributed to the presence of vacancies. Mattila and Nieminen[58] suggested that the initial state is a shallow donor-induced energy level, whereas the final state is the deep acceptor, possibly related to a cation vacancy complex. The presence of the YL band has been strongly correlated with the crystalline defects in AlN as well. Li *et al.*[59] reported on the evolution of broadband luminescence around 2.3 eV upon Mn$^+$ implantation. Similar to the oxygen-related contribution to the midgap luminescence, a straight correlation of the peak intensities to the contamination levels in the samples analyzed here could not be detected. Mason *et al.*[32] have shown that the respective emission band has been indeed generated by the radiative transitions in at least seven different native point-defect centers. One of these bands was unambiguously identified with a displacement of an ^{27}Al atom. Based on that, it can be only speculated that both nitrogen vacancies and Al interstitial

point defects could be responsible for the observed emission bands at about 2.2 eV in AlN crystals. Further theoretical and experimental analysis is needed to rule out one of them and provide an unambiguous mechanism for these transitions.

IV. CONCLUSION

The origin of the emission and absorption bands of AlN in the UV and visible spectral range was investigated by Raman, PL emission, and absorption spectroscopy. Bulk AlN crystals with different defect densities and impurity concentrations were grown by varying the growth equipment, the process parameters, and the reaction crucibles in the PVT method.

High crystalline quality, orientation, and the absence of strain in the bulk crystals were determined by Raman spectroscopy. The analysis of the PL transmission and absorption results, the PL emission behavior, and the GDMS analysis shows that oxygen and oxygen-related defects in bulk AlN crystals are not necessarily the dominant impurities. In particular, nitrogen vacancies, B, C, Si impurities were found in concentrations that may significantly influence the optical properties of AlN. The presence of nitrogen vacancies was confirmed by characteristic emission and absorption bands. However, a straight correlation of the observed emission and absorption bands to any of the mentioned elements is missing, suggesting the presence of more complex defect structures in this material system.

Despite the pronounced midgap emission, absorption edges between 5.95 and 4.1 eV (at RT) have been identified for bulk AlN. The absorption coefficients of the AlN single crystals were determined for the spectral range from 6.2 eV to 10 meV.

ACKNOWLEDGMENTS

[1] B. Monemar, J. Mater. Sci.: Mater. Electron. **10**, 227 (1999).
[2] S. Strite and H. Morkoc, J. Vac. Sci. Technol. B **10**, 1237 (1992).
[3] L. Liu and J. H. Edgar, Mater. Sci. Eng., R. **37**, 61 (2002).
[4] O. Ambacher, J. Phys. D **31**, 2653 (1998).
[5] R. Schlesser and Z. Sitar, J. Cryst. Growth **234**, 349 (2002).
[6] R. Schlesser, R. Dalmau, and Z. Sitar, J. Cryst. Growth **241**, 416 (2002).
[7] J. C. Rojo, G. A. Slack, K. Morgan, B. Roghothamachar, M. Dudley, and L. J. Schowalter, J. Cryst. Growth **231**, 317 (2001).
[8] J. Pastrnak and L. Roskovcova, Phys. Status Solidi **7**, 331 (1964).
[9] C. O. Dugger, Mater. Res. Bull. **9**, 331 (1974).
[10] G. A. Slack, and T. F. McNelly, J. Cryst. Growth **34**, 263 (1976).
[11] C. M. Balkas, Z. Sitar, T. Zheleva, L. Bergman, R. Nemanich, and R. F. Davis, J. Cryst. Growth **179**, 363 (1997).
[12] R. Schlesser, R. Dalmau, R. Yakimova, and Z. Sitar, Mater. Res. Soc. Symp. Proc. **693**, 1.9.9.1 (2001).
[13] J. C. Rojo, G. A. Slack, K. Morgan, B. Raghothamachar, M. Dudley, and L. J. Schowalter, J. Cryst. Growth **231**, 317 (2001).
[14] N. B. Singh, A. Berghmans, H. Zhang, T. Wait, R. C. Clarke, J. Zingaro, and J. C. Golombeck, J. Cryst. Growth **250**, 107 (2003).
[15] M. Gadenne, J. Plon, and P. Gadenne, Thin Solid Films **333**, 251 (1998).

[16]S. Strite and H. Morkoc, J. Vac. Sci. Technol. B **10**, 1237 (1992).

[17]S. Loughin, R. H. French, W. Y. Ching, Y. N. Xu, and G. A. Slack, Appl. Phys. Lett. **63**, 1182 (1993).

[18]D. Brunner, H. Angerer, E. Bustarret, F. Freundenberg, R. Höpler, R. Dimitrov, O. Ambacher, and M. Stutzmann, J. Appl. Phys. **82**, 5090 (1997); U. Ozgur, G. Webb-Wood, H. O. Everitt, F. Fun, and H. Morkoc, Appl. Phys. Lett. **79**, 4103 (2001).

[19]S. Yu. Karpov, A. V. Kulik, I. N. Przhevalskii, M. S. Ramm, and Yu. N. Makarov, Phys. Status Solidi C **0**, 1989 (2003).

[20]R. A. Youngman and J. H. Harris, J. Am. Ceram. Soc. **73**, 3238(1990).

[21]J. H. Harris and R. A. Youngman, in *Properties of Group III Nitrides* IEE, EMIS Datarev Series No. 11, edited by J. H. Edgar (Inspec, London, 1994), p. 203.

[22]G. A. Slack, and T. F. McNelly, J. Cryst. Growth **34**, 263 (1976).

[23]G. A. Slack, L. J. Schowalter, D. Morelli, and J. A. Freitas Jr., J. Cryst. Growth **246**, 287 (2002).

[24]M. Bickermann, B. M. Epelbaum, and A. Winnacker, Phys. Status Solidi C **0**, 1993 (2003).

[25]A. Sarua *et al.*, Mater. Res. Soc. Symp. Proc. **798**, Y5.17.1 (2004).

[26]J. A. Freitas, Jr., G. C. B. Braga, E. Silveira, J. G. Tischler, and M. Fatemi, Appl. Phys. Lett. **83**, 2584 (2003).

[27]B. Monemar, J. Cryst. Growth **189/190**, 1 (1998).

[28]M. Morita, K. Tsubouchi, and N. Mikoshiba, Jpn. J. Appl. Phys., Part 1 **21**, 1102 (1982).

[29]H. Morkoc, in *Nitride Semiconductors and Devices*, edited by R. Hull, R. M. Osgood, Jr., H. Sakaki, and A. Zunger (Springer, New York, 1999), p. 17.

[30]A. Yoshida, in *Properties, Processing and Applications of Gallium Nitride and Related Semiconductors*, EMIS Data Reviews Series No. 23, edited by J. H. Edgar, S. Strite, I. Akasaki, H. Amano, and C. Wetzel (INSPEC, London, 1999).

[31]W. M. Jadwisienczak, H. J. Lozykowski, I. Berishev, A. Bensaoula, I. G. Brown, J. Appl. Phys. **89**, 4384 (2001).

[32]P. M. Mason, H. Przybylinska, G. D. Watkins, W. J. Choyke, and G. A. Slack, Phys. Rev. B **59**, 1937 (1999).

[33]M. Schwoerer-Bohning and A. T. Macrander, J. Phys. Chem. Solids **61**, 485 (2000).

[34]U. Haboeck, H. Siegle, A. Hoffmann, and C. Thomsen, Phys. Status Solidi C **0**, 1710 (2003), and references therein.

[35]V. Yu. Davydov, *et al.*, J. Cryst. Growth **189/190**, 656 (1998).

[36]C. Carlone, K. M. Lakin, and H. R. Shanks, J. Appl. Phys. **55**, 4010 (1984).

[37]A. Goñi, H. Siegle, K. Syassen, C. Thomsen, and J.-M. Wagner, Phys. Rev. B **64**, 035205 (2001).

[38]M. Kuball, J. M. Hayes, A. D. Prins, N. W. A. van Uder, D. J. Dunstan, Y. Shi, and J. H. Edgar, Appl. Phys. Lett. **78**, 724 (2001).

[39]C. R. Bennett, B. K. Ridley, N. A. Zakhleniuk, and M. Babikar, Physica B **263–264**, 469 (1999).

[40]H. M. Tutuncu, G. P. Srivastava, and S. Duman, Physica B **316–317**, 190 (2000).

[41]V. Noveski, B. Wu, H. Zhang, R. Schlesser, S. Mahajan, S. Beaudoin, and Z Sitar, J. Cryst. Growth **264**, 369 (2004).

[42]V. Noveski, R. Schlesser, J. A. Freitas, Jr., S. Mahajan, S. Beaudoin, and Z. Sitar, Mater. Res. Soc. Symp. Proc. **798**, Y.2.8 (2004).

[43]D. G. Esaev, S. G. Matsik, M. B. M. Rinzan, A. G. Perera, H. C. Liu, and M Buchanan, J. Appl. Phys. **93**, 1879 (2003).

[44]M. Born, and E. Wolf, *Principles of Optics*, 6th ed. (Pergamon, Oxford, 1989), p. 96.

[45]G. M. Laws, E. C. Larkins, I. Harrison, C. Molloy, and D. Somerford, J. Appl. Phys. **89**, 1108 (2001).

[46]J. Pastrnak and L. Roskovcova, Phys. Status Solidi **26**, 591 (1968).

[47]W. M. Yim, E. J. Stofko, P. J. Zanzucchi, J. I. Pankove, M. Ettenberg, and S. L. Gilbert, J. Appl. Phys. **44**, 292 (1973).

[48]J. Li, K. B. Nam, M. L. Nakarmi, J. Y. Lin, H. X. Jiang, P. Carrier, and S. H. Wei, Appl. Phys. Lett. **83**, 5163 (2003).

[49]K. B. Nam, J. Li, M. L. Nakarmi, J. Y. Lin, and H. X. Jiang, Appl. Phys. Lett. **82**, 1694 (2003).

[50]A. T. Collins, E. C. Lightowler, and P. J. Dean, Phys. Rev. **158**, 833 (1967).

[51]A. Kasic, M. Schubert, B. Kuhn, F. Scholz, S. Einfeldt, and D. Hommel, J. Appl. Phys. **87**, 3720 (2001).

[52]J. H. Harris, R. A. Youngman, and R. G. Teller, J. Mater. Res. **5**, 1763 (1990).

[53]B. Berzina, L. Trinkler, E. Palcevskis, and J. Sils, Mater. Sci. Forum **239–241**, 145 (1997).

[54]X. Jiang, F. Hossain, K. Wongchotigul, and M. G. Spencer, Appl. Phys. Lett. **72**, 1501 (1998).

[55]S. Nakahata, K. Sogabe, T. Matsuura, and A. Yamakawa, J. Am. Ceram. Soc. **80**, 1612 (1997).

[56]J. Neugebauer and C. G. Van de Walle, Appl. Phys. Lett. **69**, 503 (1996).

[57]K. Saarinen, *et al.*, Phys. Rev. Lett. **79**, 3030 (1997).

[58]T. Mattila and R. M. Nieminen, Phys. Rev. B **55**, 9571 (1997).

[59]M. K. Li, C. B. Li, C. S. Liu, X. J. Fan, D. J. Fu, Y. Shon, and T. W. Kang, J. Appl. Phys. **95**, 755 (2004).